Supporting Information

Goto et al. 10.1073/pnas.1106454108

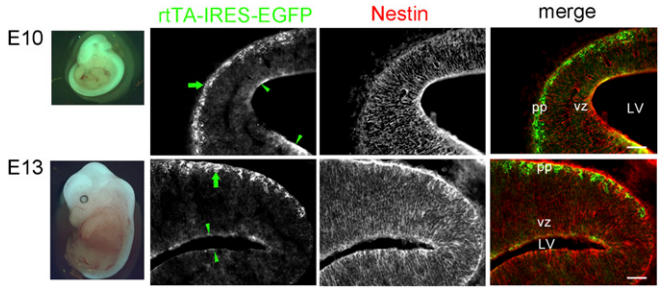

Fig. S1. Expression of the *Nes-rtTA-IRES-EGFP* transgene in embryonic neuroprogenitor cells. *Tsc1*^{cc} *Nes-rtTA*$^{+}$ embryos show EGFP fluorescent signal (*Left*) and brain sections stained with EGFP antibody (green) and nestin antibody (red) (*Right*) at E10 and E13. Note that the EGFP signal colocalizes with the nestin signal in cerebral cortical neuroepithelium of the ventricular zone (*vz*, arrowheads) and in preplate cells (*pp*, arrows). LV, lateral ventricle.

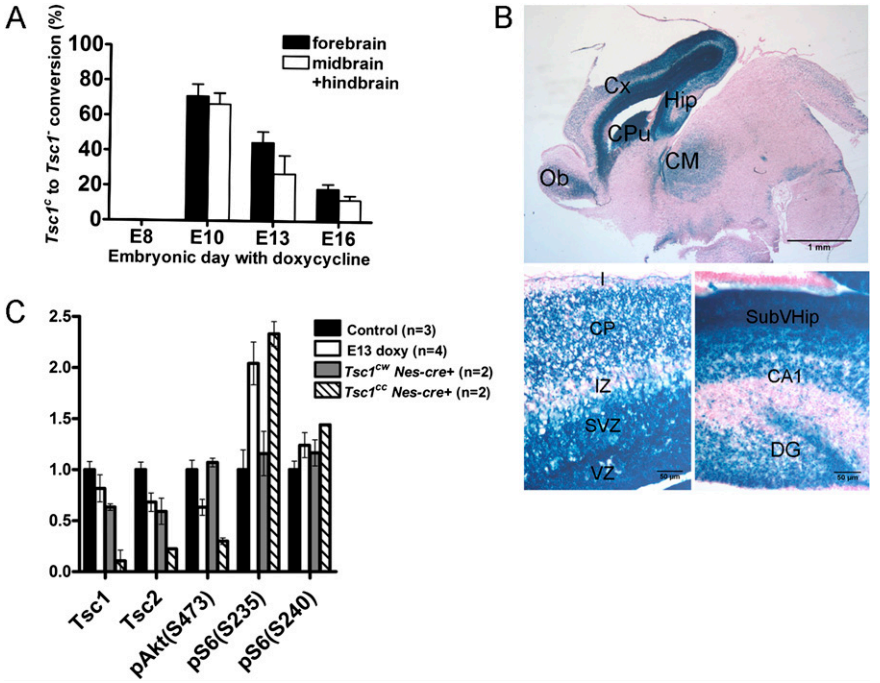

Fig. S2. Mosaic loss of Tsc1 in doxycycline-treated *Tsc1*^{cc} *Nes-rtTA*$^{+}$ *TetOP-cre*$^{+}$ mice. (*A*) Recombination at the Tsc1 floxed allele in P0 brain determined by MLPA. (*B*) LacZ staining on E16 *Tsc1*^{cc} *Nes-rtTA*$^{+}$ *TetOP-cre*$^{+}$ mutant brain 3 d after doxycycline administration at E13. (*C*) Densitometry of immunoblot analysis of P0 brain lysates. *Tsc1*^{cc} *Nes-rtTA*$^{+}$ *TetOp-cre*$^{+}$ mice showed partial loss of Tsc1 and moderate activation of the mTOR pathway in comparison to *Tsc1*^{cc} *Nestin-cre*$^{+}$ mutants. CA1, comu ammonis area 1; CP, cortical plate; DG, dentate gyrus; I, cortical layer 1; IZ, intermediate zone of cortex; SubVHip, subventricular zone of hippocampus; SVZ, subventricular zone of cortex; VZ, ventricular zone of cortex. [Scale bars: *B* (*Upper*), 1 mm; *B* (*Lower*), 50 μm.]

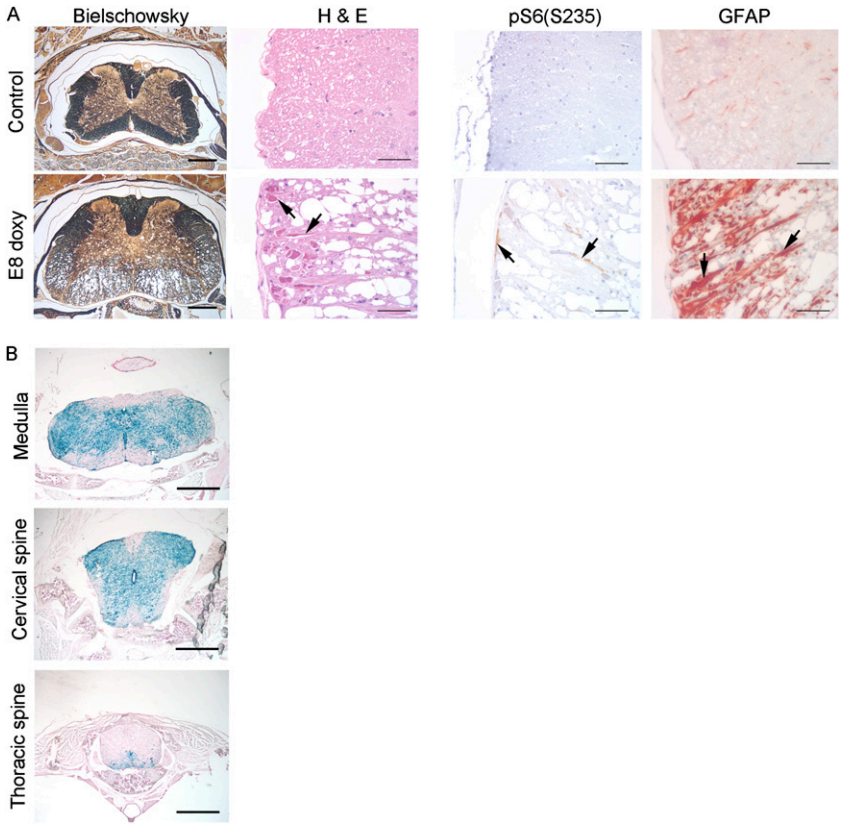

Fig. S3. White matter degeneration in upper spinal cord of *Tsc1*^{cc} *Nes-rtTA*$^{+}$ *TetOP-cre*$^{+}$ (*E8 doxy*) mice. (*A*) Vacuolated white matter in ventral column of cervical spinal cord at 9 mo of age. Mineralization (H&E) and abnormally elevated pS6(S235) levels were observed in very dense GFAP^{+} Rosenthal fiber-like glial fiber (arrows). (*B*) LacZ reporter staining in spinal cord of *Tsc1*^{cc} *Nes-rtTA*$^{+}$ *TetOP-cre*$^{+}$ (*E8 doxy*) mice. Cre expression is high in the medulla and cervical spinal cord, and it is restricted to the ventral region in thoracic cord and at lower levels. (Scale bars: *A*, 500 μm [Bielschowsky], 50 μm [H&E, pS6(S235), and GFAP]; *B*, 1,000 μm.)

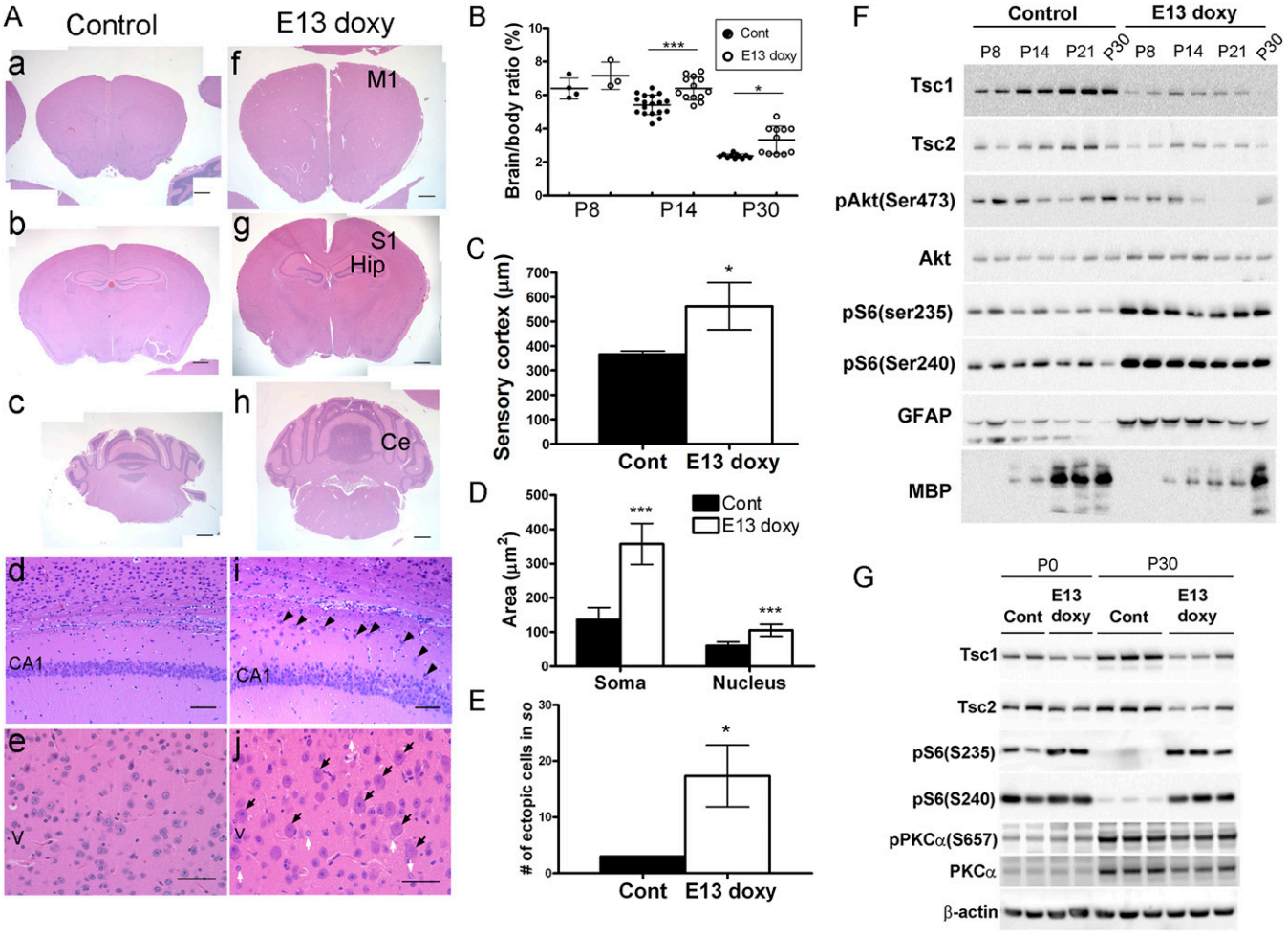

Fig. S4. Macrocephaly, hypomyelination, and gliosis in *Tsc1*^{cc} *Nes-rtTA*$^{+}$ *TetOP-cre*$^{+}$ (*E13 doxy*) mice. (*A*) Coronal brain sections of P42 control mice (*a*–*e*) and *Tsc1*^{cc} *Nes-rtTA*$^{+}$ *TetOP-cre*$^{+}$ (*E13 doxy*) mice (*f*–*j*). The cerebral cortex is greatly enlarged, including the primary motor cortex (M1) and somatosensory cortex (S1). CA1, comu ammonis area 1; Ce, cerebellum; Hip, hippocampus. (*i* and *j*) Ectopic cells in the stratum oriens (arrowheads), enlarged dysmorphic layer V neurons (black arrows), and hypertrophic astrocytes (white arrows) are indicated. (Scale bars: *A*, *a*–*c* and *f*–*h*, 500 μm; *A*, *d*, *e*, *i*, and *j*, 50 μm.) (*B*) Brain-to-body weight ratios. (*C*) Somatosensory cortex width at P42 ($n = 3$). Cont, control. (*D*) Cell (soma) and nucleus size analysis on layer V neurons in somatosensory area at P42 ($n = 20$ cells, 2 animals each). (*E*) Numbers of ectopic cells found in CA1 stratum oriens. (*F*) Reduced expression of Tsc1 and Tsc2, activation of mTORC1, and related effects during development of *Tsc1*^{cc} *Nes-rtTA*$^{+}$ *TetOP-cre*$^{+}$ (*E13 doxy*) mice. Immunoblotting of P8–P30 cerebral cortex lysates of control and mutant mice (*E13 doxy*) was performed. Tsc1, Tsc2, and pAkt levels are reduced; mTORC1 is activated (increased pS6); and GFAP levels are increased at all time points examined. Myelination (MBP) was delayed. (*G*) Reduced mTORC2 activity in the brain of *Tsc1*^{cc} *Nes-rtTA*$^{+}$ *TetOP-cre*$^{+}$ (*E13 doxy*) mice at P30. Both phospho-PKCα (S657) and total PKCα levels are decreased in young adult mutant brain. Also, note that mTORC1 activity in the normal brain is higher at birth than at P30, as assessed by pS6(S235) and pS6(S240) levels. $^{*}P < 0.05$; $^{**}P < 0.01$; $^{***}P < 0.001$.

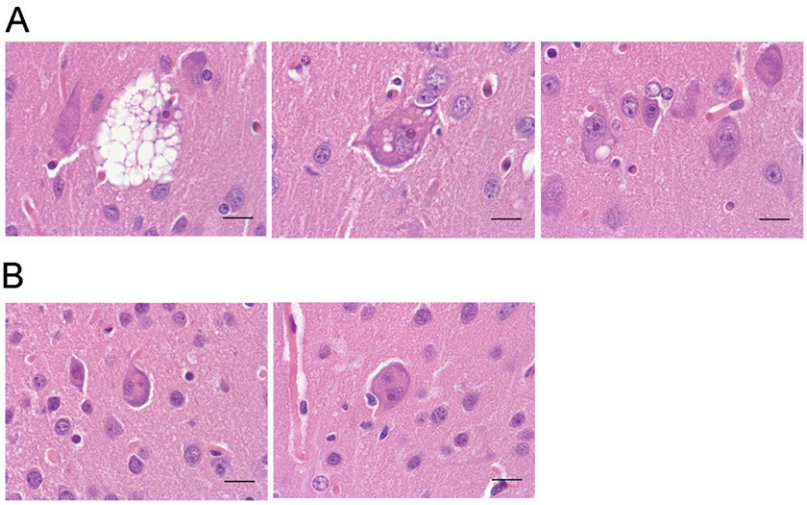

Fig. S5. Brain pathology and vacuolated giant cells in *Tsc1*^{cc} *Nes-rtTA*$^{+}$ *TetOP-cre*$^{+}$ *(E13 doxy)* mice at the age of 6 mo. (*A*) Giant cells at various stages of vacuole development (*Left* and *Center,* layer II/III; *Right,* layer V). (*B*) Binucleate cells were found in layer II/III (*Left*) and layer V (*Right*). (Scale bars: 10 μm.)

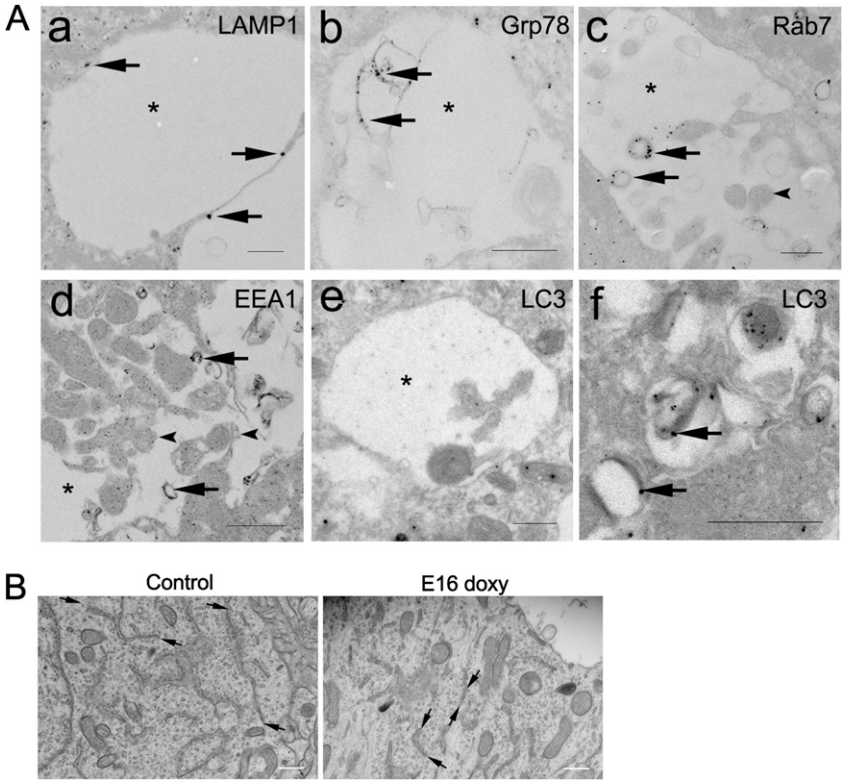

Fig. S6. Ultrastructural analysis of giant cells in *Tsc1*^{cc} *Nes-rtTA*$^{+}$ *TetOP-cre*$^{+}$ (*E16 doxy*) mice. (*A*) Localization of LAMP1 (*a*) to the endomembrane of vacuoles (arrows). Vacuoles (*) contain ER (Grp78, *b*), late endosomes (Rab7, *c*), early (EEA1, *d*) endosomes (arrows), and mitochondria (arrowheads). Vacuoles are negative for autophagy marker LC3 (*e*) and different from normal LC3^{+} autophagosomes (*f*). (*B*) Fragmented ER is seen in vacuolated giant cells in *Tsc1*^{cc} *Nes-rtTA*$^{+}$ *TetOP-cre*$^{+}$ (*E16 doxy*) mutant mice. Arrows indicate the edges of ERs. (Scale bars: *A*, *a* and *b*, 10 μm; *A*, *c*, 1 μm; *A*, *d*, 200 nm; *A*, *e* and *f*; *B*, 500 nm.)

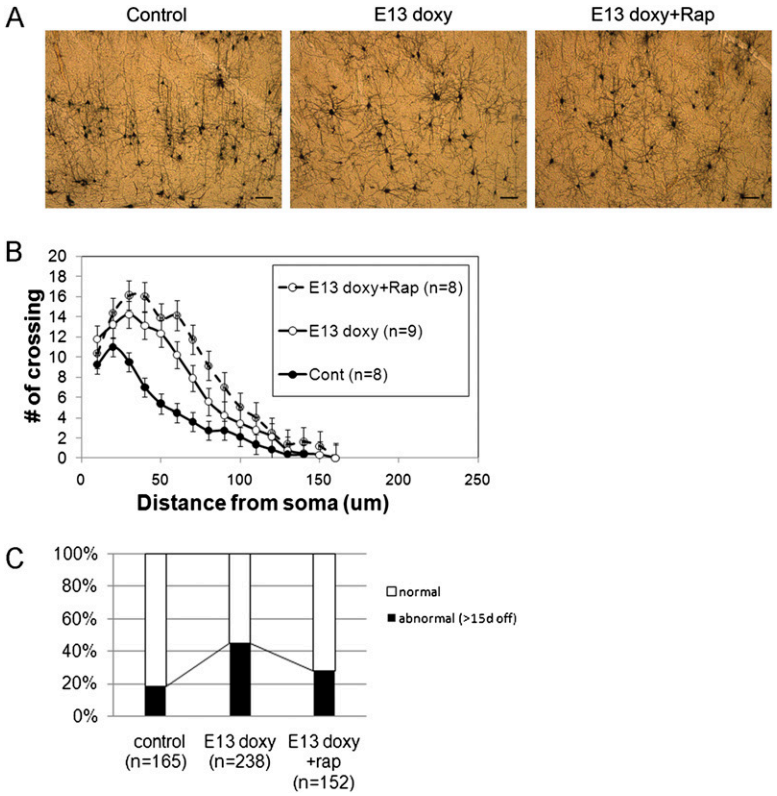

Fig. S7. Postnatal rapamycin treatment effects on dendritic morphology of cortical neurons. (*A*) Cortical brain sections of control, untreated *Tsc1*^{cc} *Nes-rtTA*$^{+}$ *TetOP-cre*$^{+}$ (*E13 doxy*) mutant, and rapamycin (Rap)-treated mutant mice by Golgi silver staining (n = 3). (Scale bars: 100 μm.) (*B*) Sholl analysis. The abnormal complex dendrite structure in the mutants was not reversed by postnatal rapamycin treatment. Rapamycin-treated mutants appeared somewhat worse, with more crossings than untreated mutants. However, only the comparison at 80 μm was statistically significant (P = 0.044). (*C*) Apical dendrite orientation. Pyramidal neurons in layer V somatosensory cortex that have an abnormal orientation (>15° angle of apical dendrite compared with a vertical line to the pia) are shown. Rapamycin treatment reduced the percentage of neurons with a cell polarity defect in the mutants.